

# GTM: General Trajectory Modeling with Auto-regressive Generation of Feature Domains

Yan Lin

School of Computer and Information Technology, Beijing Jiaotong University, Beijing, China  
ylincs@bjtu.edu.cn

Bin Yang

School of Data Science and Engineering, East China Normal University, Shanghai, China  
byang@dase.ecnu.edu.cn

Jilin Hu

School of Data Science and Engineering, East China Normal University, Shanghai, China  
jlhu@dase.ecnu.edu.cn

Shengnan Guo

School of Computer and Information Technology, Beijing Jiaotong University, Beijing, China  
guoshn@bjtu.edu.cn

Youfang Lin

Huaiyu Wan

School of Computer and Information Technology, Beijing Jiaotong University, Beijing, China  
{yflin,hywan}@bjtu.edu.cn

## ABSTRACT

Vehicle movement is frequently captured in the form of trajectories, i.e., sequences of timestamped locations. Numerous methods exist that target different tasks involving trajectories such as travel-time estimation, trajectory recovery, and trajectory prediction. However, most methods target only one specific task and cannot be generalized to other tasks. Moreover, existing methods often perform poorly on long trajectories, while also underperforming on re-sampled, sparse trajectories.

To address these shortcomings, we propose the General Trajectory Model (GTM) that aims to support different tasks based on regular and sparse trajectories without the need for retraining or extra prediction modules. GTM is designed expressly to achieve adaptability and robustness. First, GTM separates the features in trajectories into three distinct domains, such that each domain can be masked and generated independently to meet specific input and output requirements of a given task. Second, GTM is pre-trained by reconstructing densely sampled trajectories given re-sampled sparse counterparts. This process enables GTM to extract detailed spatio-temporal and road segment information from sparse trajectories, ensuring consistent performance when trajectories are sparse. Experiments involving three representative trajectory-related tasks on two real-world trajectory datasets provide insight into the intended properties performance of GTM and offer evidence that GTM is capable of meeting its objectives.

## PVLDB Reference Format:

Yan Lin, Jilin Hu, Shengnan Guo, Bin Yang, Christian S. Jensen, Youfang Lin, and Huaiyu Wan. GTM: General Trajectory Modeling with Auto-regressive Generation of Feature Domains. *PVLDB*, 14(1): XXX-XXX, 2020.  
doi:XX.XX/XXX.XX

This work is licensed under the Creative Commons BY-NC-ND 4.0 International License. Visit <https://creativecommons.org/licenses/by-nc-nd/4.0/> to view a copy of this license. For any use beyond those covered by this license, obtain permission by emailing info@vldb.org. Copyright is held by the owner/author(s). Publication rights licensed to the VLDB Endowment.

Proceedings of the VLDB Endowment, Vol. 14, No. 1 ISSN 2150-8097.  
doi:XX.XX/XXX.XX

## PVLDB Artifact Availability:

The source code, data, and/or other artifacts have been made available at <https://github.com/Logan-Lin/GTM>.

## 1 INTRODUCTION

A trajectory is a sequence of timestamped locations that captures the movement of an object. Figure 1 provides an example where a trajectory  $\mathcal{T}$  captures the travel of a vehicle from  $l_1$  to  $l_7$ . This trajectory consists of seven GPS points recorded at an interval of 30 seconds:  $\mathcal{T} = \langle (l_1, t_1), (l_2, t_2), \dots, (l_7, t_7) \rangle$ , where  $t_i - t_{i-1} = 30$  seconds for  $i \in \{2, 3, \dots, 7\}$ . Substantial spatio-temporal information can be mined from this trajectory, e.g., 1) the travel time of the trip,  $t_7 - t_1$ ; 2) the road segments that the trip visited; 3) the average travel speed on each road segment, which can reflect travel conditions; 4) accelerations and decelerations that capture driving behavior. Such information provides a rich foundation for analyzing the movement patterns of individual vehicles and traffic patterns on road networks, which in turn powers various important tasks in Intelligent Transportation System (ITS). These tasks include trajectory prediction [10, 11, 24, 29], travel time estimation [12, 15, 34, 53], anomaly detection [16, 31], and trajectory clustering [9, 25, 49, 54].

Given the rich spatio-temporal information that trajectories can provide and their applicability across multiple tasks, the same set of trajectories is often utilized for various tasks simultaneously. Traditionally, individual models are created and trained for each specific task. Thus, these models often solely concentrate on task-specific information, which hinders their adaptability to other tasks and potentially restricts their effectiveness. Moreover, training and storing multiple models for different tasks adversely affect computational and storage efficiency. Consequently, there is a pressing need to develop a general trajectory model that can be trained once on a dataset and effectively address various tasks.

Several existing studies [13, 21, 26, 50] have introduced general trajectory models through representation learning techniques. These methods commonly involve training a trajectory encoder,

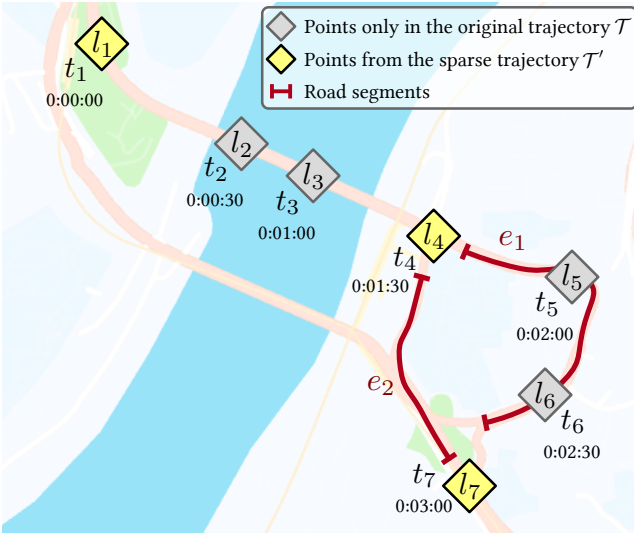


Figure 1: A trajectory and its re-sampled counterpart.

which maps each trajectory to an embedding vector. However, utilizing the embedding vector alone is insufficient for most tasks. To make task-specific predictions, supplementary prediction modules must be connected to the embedding vector, which requires additional fine-tuning processes. Apart from the need for fine-tuning, existing methods suffer from two significant shortcomings that prevent them from fully achieving the objective of constructing a general trajectory model.

**First, existing methods face limitations in adapting to different types of tasks due to the requirement of the integrity of a trajectory’s features.** There is a wide range of trajectory-related tasks that involve varying arrangements of input and output features. Some tasks, especially, do not require the inclusion of every feature from all points in a trajectory. For instance, in origin-destination travel time estimation [30], only the origin, destination, and departure time of a trajectory are known prior to its occurrence. Similarly, in trajectory recovery [8], there are often long spans of missing trajectory points among the known ones.

Existing methods typically have strict requirements regarding the integrity of the input features in order to function properly. Specifically, they commonly specify that the spatial and temporal features of all points in a trajectory be provided as input. For example, t2vec [26] requires the coordinate and timestamp of each trajectory point, while Trembr [13] and START [21] necessitate the road segment and timestamp for each point. Consequently, these methods are unable to adapt to tasks such as travel time estimation and trajectory recovery, where the requirement of the integrity of a trajectory’s features cannot be fulfilled.

**Second, existing methods scale poorly with long vehicle trajectories and underperform on re-sampled sparse trajectories.** In real-world settings, vehicle locations are often sampled at high rates, resulting in long vehicle trajectories. State-of-the-art methods, including PreCLN [55] and START [21], utilize Transformer-based [39] trajectory encoders to capture long-term correlations in these trajectories. However, Transformers exhibit

poor scalability with long trajectories due to their quadratic complexity,  $O(N^2)$ , in the trajectory length  $N$ . Additionally, the data storage requirements for these lengthy trajectories are substantial.

To address these issues, a common approach is to re-sample the original trajectories into sparser ones with larger sampling intervals to enhance computational and storage efficiency. However, existing methods encounter performance issues when working with such sparse trajectories as they struggle to address the information loss caused by the sparsity properly. For example, in Figure 1, a sparse trajectory  $\mathcal{T}' = \{(l_1, t_1), (l_4, t_4), (l_7, t_7)\}$  is re-sampled from the original trajectory  $\mathcal{T}$  with a sampling interval of 90 seconds. When existing methods are fed with  $\mathcal{T}'$  as input, they tend to overlook spatio-temporal information not explicitly captured in  $\mathcal{T}'$ , such as the deceleration between points  $(l_2, t_2)$  and  $(l_3, t_3)$ . The sparsity also amplifies uncertainty in the road segment features, thereby negatively affecting the performance of methods that rely on these features. For example, distinguishing whether the vehicle traverses road segment  $e_1$  or  $e_2$  between points  $(l_4, t_4)$  and  $(l_7, t_7)$  poses a challenge for existing methods.

To this end, we propose the *General Trajectory Model (GTM)*. GTM can be trained once and adapted to effectively handle various trajectory-related tasks, facilitating its adaptability and efficiency in ITS applications. To ensure its adaptability, we divide the features in trajectories into three distinct domains. Each domain can be masked and generated independently to meet the specific input and output requirements of the task at hand. Furthermore, GTM consistently demonstrates strong performance when faced with sparse trajectories. To enhance GTM’s robustness to sparsity, we pre-train GTM to enable it to extract spatio-temporal and road segment features embedded in the densely sampled trajectories, even when presented with only the sparsely re-sampled ones. The primary contributions of the paper are as follows.

- We propose the GTM, a versatile and robust general trajectory model. GTM can be trained once and effectively adapt to multiple trajectory-related tasks without additional prediction modules, even when confronted with sparse trajectories.
- We separate the features in trajectories into three domains, allowing each domain to be masked and generated separately based on the specific input and output requirements of the task. This flexibility enables the GTM to adapt to various types of tasks.
- We pre-train GTM by reconstructing densely sampled trajectories using their re-sampled sparse counterparts. This process enhances GTM’s robustness to sparsity and maintains its performance on sparse trajectories.
- We conduct extensive experimental study on two real-world datasets and three representative tasks, offering insight into the performance properties of the proposed model, and providing evidence that the model is capable of meeting its design goals.

## 2 RELATED WORK

### 2.1 Task-specific Trajectory Models

Task-specific models are designed and trained for specific tasks. These models are commonly used for trajectory-related tasks due to their ease of implementation.

For travel time estimation, path-based approaches including WDR [43], DeepTTE [40], DeepETA [44], WDDRA [14], and DRTTE [48]

predict travel times based on the given travel paths. On the other hand, origin-destination-based approaches including TEMP [41], ST-NN [22], MURAT [27], DeepOD [53], and DOT [30] estimate travel times by considering the origin, destination, and departure time. For trajectory recovery, TrImpute [8] is a non-learning-based method. In contrast, AttnMove [45], MTrajRec [35], and RNTrajRec [5] are learning-based methods built on the seq2seq framework [36]. For trajectory prediction, models like DeepMove [11], HST-LSTM [24], and ACN [32] leverage recurrent neural networks [18] to capture sequential patterns in trajectories. PreCLN [46] integrates contrastive learning [4] to improve prediction accuracy.

While task-specific trajectory models have their advantages, their adaptability and computational efficiency are limited in ITS applications. Models tailored to specific tasks cannot be easily repurposed for other tasks, leading to the need for separate models for each task, which can adversely affect computational resources and storage efficiency.

## 2.2 General Trajectory Models

In response to the limitations of task-specific models, there is a growing interest in general trajectory models that can accommodate multiple tasks.

Among these models, trajectory2vec [52] constructs behavior sequences from trajectories to extract key information and then utilizes an auto-encoding framework [17] to compress each sequence into an embedding vector. t2vec [26] employs a denoising auto-encoding framework to enhance its resilience to trajectory noise. Trembr [13] leverages auto-encoding techniques to extract road network and temporal information embedded in trajectories effectively. SML [55] integrates the contrastive predictive coding framework [38], providing an innovative method for learning embedding vectors for trajectories. START [21] introduces a comprehensive approach to trajectory embedding learning by combining masked language model [6] and SimCLR [4] to enhance its learning capability.

While these general trajectory models exhibit versatility, they often require additional prediction modules to generate task-specific predictions based on their output embedding vectors. Moreover, they are limited in the variety of tasks they can adapt to and will experience performance degradation when confronted with sparse trajectories. These limitations hinder the realization of a truly comprehensive general trajectory model.

## 3 PRELIMINARIES

### 3.1 Definitions

**DEFINITION 1 (ROAD NETWORK).** A road network is modeled as a directed graph  $\mathcal{G} = (\mathcal{V}, \mathcal{E})$ , where  $\mathcal{V}$  is a set of nodes, each node  $v_i \in \mathcal{V}$  models an intersection between road segments or the end of a segment, and  $\mathcal{E}$  is a set of edges, each edge  $e_i \in \mathcal{E}$  models a road segment linking two nodes. An edge is given by starting and ending nodes:  $e_i = (v_j, v_k)$ .

**DEFINITION 2 (TRAJECTORY).** A trajectory  $\mathcal{T}$  is a sequence of timestamped point locations:  $\mathcal{T} = \langle (l_1, t_1), (l_2, t_2), \dots, (l_{|\mathcal{T}|}, t_{|\mathcal{T}|}) \rangle$ , where  $l_i = (l_i^{\text{long}}, l_i^{\text{lat}})$  are the spatial coordinates of the  $i$ -th location,

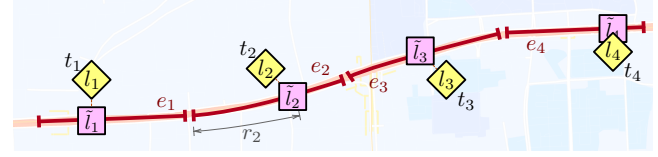


Figure 2: A trajectory and its map-matched counterpart.

$l_i^{\text{long}}$  and  $l_i^{\text{lat}}$  denote longitude and latitude, respectively, and timestamp  $t_i$  is the time at which  $l_i$  is visited.

**DEFINITION 3 (SAMPLING INTERVAL).** A trajectory's sampling interval  $\eta$  is the time interval between its consecutive points, i.e.,  $\eta = t_i - t_{i-1}$ ,  $i \in \{2, 3, \dots, |\mathcal{T}|\}$ . Given a trajectory that is originally densely sampled, its sparse counterpart can be obtained by re-sampling the trajectory with a larger interval  $\mu$ .

It is important to note that we assume consistent sampling intervals to ensure consistency in the experimental evaluation. Nevertheless, the proposed model can be applied to trajectories with varying sampling intervals.

**DEFINITION 4 (MAP-MATCHED TRAJECTORY).** By using a map-matching algorithm [2], a trajectory  $\mathcal{T}$  can be projected onto the underlying road network  $\mathcal{G}$ . The map-matched trajectory can be denoted as  $\tilde{\mathcal{T}} = \langle (\tilde{l}_1, t_1), (\tilde{l}_2, t_2), \dots, (\tilde{l}_{|\mathcal{T}|}, t_{|\mathcal{T}|}) \rangle$ , where  $\tilde{l}_i = (e_i, r_i)$ ,  $e_i \in \mathcal{E}$  is the map-matched road segment occupied by location  $l_i$ , and  $r_i$  is the fraction of the length of the road segment traveled by time  $t_i$ .

**EXAMPLE 1.** Figure 2 gives an example of a trajectory  $\mathcal{T} = \langle (l_1, t_1), (l_2, t_2), (l_3, t_3), (l_4, t_4) \rangle$ , where the locations are denoted in diamonds. Map-matching yields map-matched trajectory  $\tilde{\mathcal{T}} = \langle (\tilde{l}_1, t_1), (\tilde{l}_2, t_2), (\tilde{l}_3, t_3), (\tilde{l}_4, t_4) \rangle$ , where the locations are in squares. For example,  $l_2$  is map-matched onto  $\tilde{l}_2$ , which is in the middle of road segment  $e_2$ . Thus, we use  $r_2$  to denote the fraction of the length of  $e_2$  that the vehicle has traveled, resulting in  $\tilde{l}_2 = (e_2, r_2)$ .

## 3.2 Problem Statement

**General Trajectory Modeling.** The objective is to construct a general trajectory model  $f_\theta$ , where  $\theta$  denotes a set of learnable parameters. During evaluation,  $f_\theta$  takes a certain arrangement of trajectory  $\mathcal{T}$  as input and generates an output tailored to the particular task at hand, denoted as  $\hat{Y} = f_\theta(\text{arrange}(\mathcal{T}))$ . For example, for travel time estimation,  $\text{arrange}(\mathcal{T})$  extracts the origin, destination, and departure time of  $\mathcal{T}$ , and  $\hat{Y}$  is the estimated travel time; for trajectory prediction,  $\text{arrange}(\mathcal{T})$  retains the historical part of  $\mathcal{T}$ , and  $\hat{Y}$  is the predicted future part of  $\mathcal{T}$ .

## 4 METHODOLOGY

### 4.1 Overall Framework

The overall framework of the proposed GTM is illustrated in Figure 3. We first divide the trajectory features into three distinct domains: spatial, temporal, and road segment, as depicted in Figure 3(a). Each point in the trajectory can be represented as a tuple consisting of these three domains. We refer to the tuple representing the  $i$ -th point in the trajectory  $\mathcal{T}$  as  $g_i^{\mathcal{T}}$ .

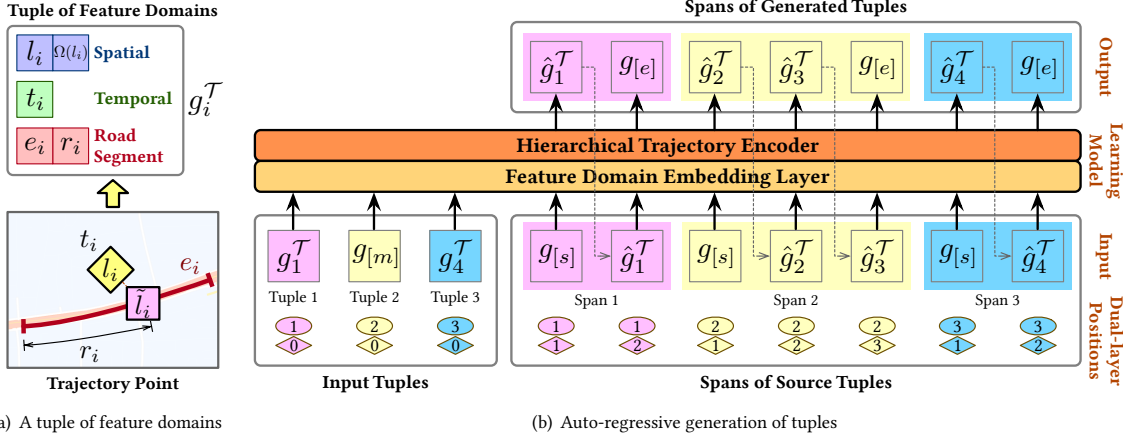


Figure 3: Overall framework.

Each feature domain in  $g_i^T$  can be masked and generated independently. Specifically, a domain can be replaced with a special mask token to indicate that it needs to be generated. Additionally, the tuple  $g_{[m]}$ , filled with the mask token, can represent all feature domains of a sub-trajectory that require generation. For each input tuple containing the mask token, a series of tuples is auto-regressively generated, creating a *span* of generated tuples. This generation process begins with a tuple  $g_{[s]}$  filled with a special start token added to the input, and proceeds iteratively by adding the last generated tuple to the input to produce the next generated tuple. The process concludes when a tuple  $g_{[e]}$  filled with a special end token is produced. Figure 3(b) provides an example where three spans are generated corresponding to the three input tuples. The flexibility provided by the above design enables GTM to adapt to various tasks, as it can accept task-specific input arrangements and generate the desired output.

To facilitate the model’s ability to extract information and correlations from feature domains, we introduce the feature domain embedding layer and the hierarchical trajectory encoder. Additionally, to enhance the model’s robustness to sparse trajectories, the learnable parameters in the model are pre-trained by reconstructing the feature domains of densely sampled trajectories given their re-sampled sparse counterparts. The next sections detail designs and modules in the proposed GTM.

## 4.2 Feature Domains

In order to improve the model’s ability to handle different tasks, the features in trajectories are divided into three domains. Each domain can be masked and generated separately, depending on the specific input and output requirement of the respective task.

**4.2.1 Tuple of Feature Domains.** Given the  $i$ -th point  $(l_i, t_i)$  of trajectory  $\mathcal{T}$ , we split its features into three domains: spatial, temporal, and road segment.

The spatial domain contains features related to the coordinate  $l_i$ . These features include  $l_i$  itself, and a set  $\Omega(l_i)$  of road segments located within a distance of  $\delta$  meters from  $l_i$ .  $\Omega(l_i)$  enhances the model’s understanding of the relationship between coordinates and road segments.

The temporal domain contains the timestamp  $t_i$  measured in seconds. To standardize  $t_i$ , we subtract it from the initial timestamp  $t_0$  of the trajectory.

The road segment domain consists of road segment  $e_i$  and fraction  $r_i$  from  $\tilde{l}_i$ , which can be obtained through map-matching the coordinate  $l_i$  following Definition 4.

Finally, we transform  $(l_i, t_i)$  into a *tuple* consisting of the above three domains as:

$$g_i^T = ((l_i, \Omega(l_i)), t_i, (e_i, r_i)) \quad (1)$$

**4.2.2 Auto-regressive Generation.** To generate a feature domain in the tuple  $g_i^T$ , we fill that domain with the mask token  $[m]$ , denoting a masked domain. This tuple is then provided to the model as input. Next, the masked domain is generated through an auto-regressive process, where each input tuple corresponds to a series of generated tuples refer to as a *span*. The generation begins by adding a tuple  $g_{[s]} = ([s], [s], [s])$  with all domains filled with the start token  $[s]$  to the input. The model then outputs the generated tuple  $\hat{g}_i^T$ . Subsequently,  $\hat{g}_i^T$  is added back to the input. Finally, the model outputs a tuple  $g_{[e]} = ([e], [e], [e])$  with all domains filled with the end token  $[e]$ , indicating the completion of the generation. An example of this generation process can be observed in the input tuple  $g_1^T$  and the generated span  $\langle \hat{g}_1^T, g_{[e]} \rangle$  in Figure 3(b).

In cases where all feature domains of a sub-trajectory need to be generated, this sub-trajectory is replaced by a single tuple  $g_{[m]} = ([m], [m], [m])$  with all domains filled with the mask token  $[m]$ . The generation follows a similar auto-regressive process as described above, with the distinction that the generation process is iterated by appending the previously generated tuple to the input to derive the subsequent generated tuple. The end of the generation is determined by the model itself, i.e., the output of the tuple  $g_{[e]}$ . An example of this generation process can be observed in the input tuple  $g_{[m]}$  and the generated span  $\langle \hat{g}_2^T, \hat{g}_3^T, g_{[e]} \rangle$  in Figure 3(b). This design further enhances the model’s flexibility, particularly in tasks such as trajectory recovery and trajectory prediction, where the length of the trajectory that needs to be generated cannot be predetermined.

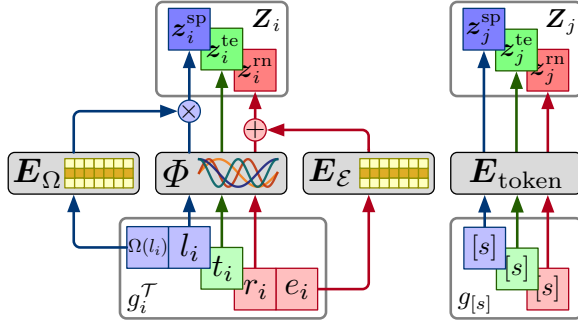


Figure 4: The feature domain embedding layer.

When multiple input tuples with masked domains are provided, these tuples are organized into an input sequence for the model. Next, the model generates the spans sequentially, with each span being generated following the above described procedures. Figure 3(b) provides an example, where the three spans corresponding to the three input tuples are sequentially generated.

**4.2.3 Dual-layer Positions.** Since each input tuple  $g_i^T$  corresponds to a span of generated tuples, we follow the practice of GLM [7] and employ dual-layer positions.

The first layer of positions, denoted as  $\mathcal{P}_i^1$ , indicates the relationship between each input tuple  $g_i^T$  and the span of generated tuples. Specifically, both  $g_i^T$  and its corresponding span of generated tuples have the same first layer positions, which is  $i$ .

The second layer of positions, denoted as  $\mathcal{P}_i^2$ , represents the order of tuples within each span of generated tuples. For  $g_i^T$ , the second layer position is always 0. Conversely, for the span of generated tuples of length  $N$ , the positions are sequentially numbered starting from 1 up to  $N$ .

**4.2.4 Feature Domain Embedding Layer.** To enhance the model’s ability to extract information from the three feature domains of each tuple, we propose an embedding layer that projects domains into the latent space, as illustrated in Figure 4.

The continuous features in the tuple  $g_i^T$ , i.e.,  $l_i^{\text{lng}}$ ,  $l_i^{\text{lat}}$ ,  $t_i$ , and  $r_i$ , exhibit periodic characteristics. To mirror these characteristics, we encode these continuous features by drawing inspiration from the learnable Fourier features [28, 37], leveraging the cyclic nature of trigonometric functions. Given an input continuous feature  $x \in \mathbb{R}$ , the encoding module  $\Phi$  projects it onto a  $d$ -dimensional latent space, defined as follows:

$$\Phi(x) = W_\Phi [\cos(xv_\Phi) \parallel \sin(xv_\Phi)], x \in \{l_i^{\text{lng}}, l_i^{\text{lat}}, t_i, r_i\}, \quad (2)$$

where  $v_\Phi \in \mathbb{R}^{d/2}$  represents a learnable projection vector, and  $W_\Phi \in \mathbb{R}^{d \times d}$  denotes a learnable projection matrix. Importantly, distinct sets of  $v_\Phi$  and  $W_\Phi$  are utilized for the four types of continuous features.

On the other hand, segment  $e_i$ , the segments in  $\Omega(l_i)$ , and the special tokens  $\{[m], [s], [e]\}$  are discrete features. For these, we employ an index-fetching embedding module for each feature. These modules involve learnable matrices  $E_\mathcal{E} \in \mathbb{R}^{|\mathcal{E}| \times d}$ ,  $E_\Omega \in \mathbb{R}^{|\mathcal{E}| \times d}$ , and  $E_{\text{token}} \in \mathbb{R}^{3 \times d}$ . The embedding vector for a discrete feature is retrieved as the corresponding row vector from these matrices. For

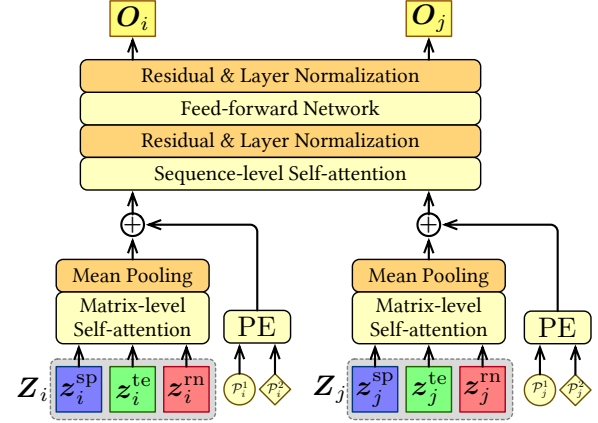


Figure 5: The hierarchical trajectory encoder.

example, the embedding vector of road segment  $e_i$  is obtained as the  $e_i$ -th row vector from  $E_\mathcal{E}$ , denoted as  $E_\mathcal{E}(e_i)$ .

Finally, the above embedding vectors are gathered to form a embedding matrix for the tuple  $g_i^T$ . Formally, the embedding vectors for the spatial, temporal, and road network domains of  $g_i^T$  are calculated as follows:

$$\begin{aligned} z_i^{\text{sp}} &= \Phi(l_i^{\text{lng}}) + \Phi(l_i^{\text{lat}}) \\ z_i^{\text{sp}} &= z_i^{\text{sp}} + \text{MultiHead}(z_i^{\text{sp}}, E_\Omega(l_i), E_\Omega(l_i)) \\ z_i^{\text{te}} &= \Phi(t_i) \\ z_i^{\text{rn}} &= E_\mathcal{E}(e_i) + \Phi(r_i) \end{aligned} \quad (3)$$

Here, MultiHead represents the dot-product attention defined in the Transformer [39], with  $N_h$  attention heads.  $E_\Omega(l_i)$  denotes the set of embedding vectors for all segments in  $\Omega(l_i)$ . In scenarios where any feature domain is one of the special tokens, the embedding vector of that domain is the embedding vector of the corresponding special token. Finally, the embedding matrix for the tuple  $g_i^T$  is expressed as  $Z_i = \langle z_i^{\text{sp}}, z_i^{\text{te}}, z_i^{\text{rn}} \rangle \in \mathbb{R}^{3 \times d}$ .

### 4.3 Hierarchical Trajectory Encoder

To model the correlations between different tuples in a trajectory and to execute the generation process described in Section 4.2.2, we propose a trajectory encoder that takes a sequence of matrices  $Z_i$  and generates a sequence of tuples  $\hat{g}_i^T$  as output.

**4.3.1 Hierarchical Attention.** To extract the correlations between the feature domains of a tuple, we take the embedding matrix  $Z_i$  and apply a matrix-level self-attention mechanism. This mechanism, along with mean pooling and position encoding, allows us to obtain the hidden state  $\mathbf{h}_i$  of the tuple. Formally:

$$\mathbf{h}_i = \text{Mean}(\text{MultiHead}(Z_i, Z_i, Z_i)) + \text{PE}(\mathcal{P}_i^1) + \text{PE}(\mathcal{P}_i^2), \quad (4)$$

where  $\mathbf{h}_i$  is the hidden state of the  $i$ -th tuple,  $Z_i$  is treated as a sequence of length 3, and PE represents the positional encoding from the Transformer [39].

Performing the generation process described in Section 4.2.2 involves a sequence of tuples provided as input. We obtain the hidden state of each tuple in the sequence using Equation 4, resulting in a sequence  $\mathbf{H} = \langle \mathbf{h}_1, \mathbf{h}_2, \dots \rangle$  of hidden states. Then, we extract

the correlations between different tuples in the sequence using a sequence-level self-attention mechanism. This mechanism incorporates a residual connection, layer normalization, and a feed-forward network. Formally:

$$\begin{aligned} H' &= \text{MultiHead}(H, H, H) \\ O' &= \text{LayerNorm}(H' + H) \\ O &= \text{LayerNorm}(\text{FFN}(O') + O'), \end{aligned} \quad (5)$$

where  $O$  represents the sequence of output states and FFN is the feed-forward network composed of two fully connected layers.

**4.3.2 Output Layer.** To generate the tuple of feature domains from the  $i$ -th output state  $O_i$ , we utilize four fully connected networks to establish an output layer. Formally:

$$\begin{aligned} \hat{l}_i &= W_c O_i + b_c \\ \hat{t}_i &= W_t O_i + b_t \\ \hat{e}_i &= \text{argmax}(p(\hat{e}_i)), p(\hat{e}_i) = \text{Softmax}(W_e O_i + b_e) \\ \hat{r}_i &= W_r O_i + b_r, \end{aligned} \quad (6)$$

where  $W_c \in \mathbb{R}^{2 \times d}$ ,  $W_t \in \mathbb{R}^{1 \times d}$ ,  $W_e \in \mathbb{R}^{(|\mathcal{E}|+1) \times d}$ , and  $W_r \in \mathbb{R}^{1 \times d}$  denote the projection matrices, while  $b_c \in \mathbb{R}^2$ ,  $b_t \in \mathbb{R}$ ,  $b_e \in \mathbb{R}^{(|\mathcal{E}|+1)}$ , and  $b_r \in \mathbb{R}$  are biases. The generated tuple is then formed as:

$$\hat{g}_i^{\mathcal{T}} = ((\hat{l}_i, \Omega(\hat{l}_i)), \hat{t}_i, (\hat{e}_i, \hat{r}_i)) \quad (7)$$

If  $\hat{e}_i = [e]$ , we denote  $\hat{g}_i^{\mathcal{T}} = g_{[e]}$ .

Given the ground truth tuple  $g_i^{\mathcal{T}}$ , we can supervise the generated tuple  $\hat{g}_i^{\mathcal{T}}$  with the following loss function:

$$\mathcal{L}_i = \mathbb{1}_i^{[e]} \left( \frac{1}{2} \|\hat{l}_i - l_i\|_2 + \|\hat{t}_i - t_i\|_2 + \|\hat{r}_i - r_i\|_2 \right) - \log p(\hat{e}_i), \quad (8)$$

where  $\mathbb{1}_i^{[e]}$  equals 0 if  $g_i^{\mathcal{T}} = g_{[e]}$  and equals 1 otherwise.

#### 4.4 Pre-training

In order to improve the model's ability to handle sparsity, we propose pre-training the model by reconstructing feature domains in densely sampled trajectories based on their re-sampled sparse counterparts. This approach allows the model to extract detailed spatio-temporal and road segment information from dense trajectories, even when only sparse trajectories are given. Consequently, the model can maintain its performance when dealing with sparse trajectories that have varying sampling intervals.

**4.4.1 Reconstruction Procedure.** Initially, a dense trajectory  $\mathcal{T}$  is selected from the dataset, where its sampling interval  $\eta$  is no longer than 15 seconds. The Fast Map Matching (FMM) algorithm [47] is then applied to obtain the trajectory's map-matched counterpart  $\tilde{\mathcal{T}}$ . Simultaneously, to emulate sparse trajectories with longer sampling intervals,  $\mathcal{T}$  is resampled at an interval  $\mu$ , where  $\mu > \eta$  and  $\mu$  is divisible by  $\eta$ , to derive a sparse counterpart  $\mathcal{T}'$ . This process is formulated as follows:

$$\mathcal{T}' = \langle (l_1, t_1), (l_{1+\mu/\eta}, t_{1+\mu/\eta}), (l_{1+2\mu/\eta}, t_{1+2\mu/\eta}), \dots, (l_{|\mathcal{T}'|}, t_{|\mathcal{T}'|}) \rangle \quad (9)$$

Notice that the last trajectory point in  $\mathcal{T}$  is retained in  $\mathcal{T}'$  to maintain the integrity of the re-sampled trajectory.

Comparing the trajectory point  $(l_i, t_i)$  in  $\mathcal{T}'$  to the corresponding point  $(\tilde{l}_i, t_i)$  in  $\tilde{\mathcal{T}}$ , the road segment domain is absent and

needs to be generated. This can be represented by a tuple  $g_i^{\mathcal{T}'} = ((l_i, \Omega(l_i)), t_i, [m])$ . On the other hand, the sub-trajectory of  $\mathcal{T}$  that lies between each pair of consecutive points in  $\mathcal{T}'$  also requires generation. This can be denoted by the tuple  $g_{[m]}$ .

The objective is to reconstruct the missing feature domains in  $\mathcal{T}'$ , which involves generating all feature domains in  $\mathcal{T}$ . To achieve this, a sequence:

$$\text{input} = \langle g_1^{\mathcal{T}'}, g_{[m]}, g_{1+\mu/\eta}, g_{[m]}, g_{1+2\mu/\eta}, \dots, g_{|\mathcal{T}'|}^{\mathcal{T}'} \rangle \quad (10)$$

consisting of tuples mentioned above is provided as the input sequence to the model. Next, the model generates a span for each tuple in the input sequence, following the process described in Section 4.2.2. Specifically, for the input tuple  $g_i^{\mathcal{T}'}$ , the model generates the span  $\langle \hat{g}_i^{\mathcal{T}'}, g_{[e]} \rangle$ . Conversely, for the input tuple  $g_{[m]}$ , the model generates the span representing the sub-trajectory in  $\mathcal{T}$  occurring between the pair of consecutive points in  $\mathcal{T}'$ , with the tuple  $g_{[e]}$  at the end.

To allow the model to extract bi-directional correlations from  $\mathcal{T}$ , we generate the spans of tuples with a shuffled order of the spans [51]. The shuffled spans are then generated sequentially, with the head and tail of each span concatenated together as a sequence. For example, the sequence:

$$\text{output} = \langle \hat{g}_j^{\mathcal{T}'}, \hat{g}_{j+1}^{\mathcal{T}'}, g_{[e]}, \hat{g}_i^{\mathcal{T}'}, \hat{g}_{i+1}^{\mathcal{T}'}, g_{[e]} \rangle \quad (11)$$

consisting of spans of generated tuples is the output of the model for one pre-training sample, with the generation order of  $\langle \hat{g}_j^{\mathcal{T}'}, \hat{g}_{j+1}^{\mathcal{T}'}, g_{[e]} \rangle$  first, followed by  $\langle \hat{g}_i^{\mathcal{T}'}, \hat{g}_{i+1}^{\mathcal{T}'}, g_{[e]} \rangle$ . Additionally, we apply a causal mask on the MultiHead in Equation 5 to prevent information leakage.

**4.4.2 Optimization Objective.** Given a dense trajectory dataset  $\mathbb{T}$ , where the sampling interval of each trajectory is below 15 seconds, we employ a variety of re-sampling intervals to create multiple sparse trajectories from each dense trajectory. This process enhances the model's ability to handle trajectories with varying sampling intervals. During pre-training, we use three re-sample intervals: 1 minute, 2 minutes, and 4 minutes.

Each pair of dense trajectory  $\mathcal{T}$  and its sparsely re-sampled counterpart  $\mathcal{T}'$  serves as a pre-training sample in Section 4.4.1. By utilizing the loss function in Equation 8, the loss function  $\mathcal{L}_{\mathcal{T}}$  of each pre-training sample can be calculated as the average of the loss  $\mathcal{L}_i$  for all generated tuples corresponding to the dense trajectory  $\mathcal{T}$ . Finally, during the pre-training process, the optimization objective is to minimize the sum of the loss  $\mathcal{L}_{\mathcal{T}}$  across all pre-training samples constructed earlier. Formally:

$$\underset{\theta}{\text{argmax}} \sum_{\mu \in \{1\text{min}, 2\text{min}, 4\text{min}\}} \sum_{\mathcal{T} \in \mathbb{T}} -\mathcal{L}_{\mathcal{T}}, \quad (12)$$

where  $\theta$  denotes the set of learnable parameters in the model.

#### 4.5 Task Adaptation

The model's flexibility allows it to adapt to various trajectory-related tasks after pre-training. We provide three representative tasks as examples.

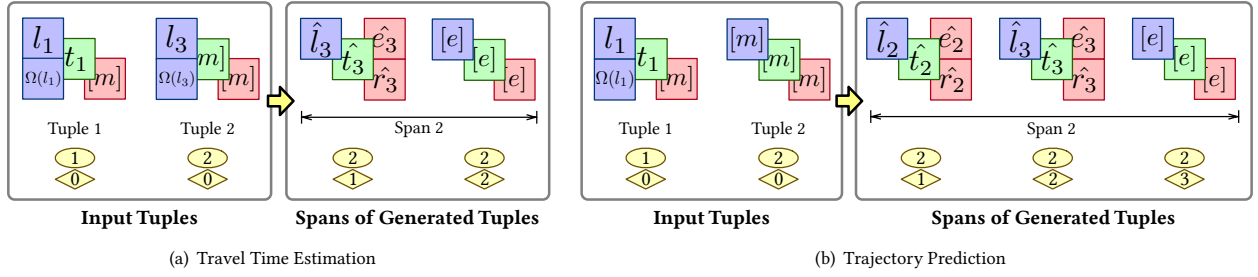


Figure 6: Unique input and output arrangements for different tasks.

**4.5.1 Travel Time Estimation (TTE).** We adopt the origin-destination-based variant of the TTE task, which involves estimating the travel time of a trajectory given only its origin  $l_o$ , destination  $l_d$ , and the departure time  $t_o$ . The model is provided with an input sequence  $\langle (l_o, t_o, [m]), (l_d, [m], [m]) \rangle$ . Next, the model generates the span corresponding to the input tuple  $(l_d, [m], [m])$  following the procedure outlined in Section 4.2.2. The generated span is expressed as  $\langle ((\hat{l}_d, \Omega(\hat{l}_d)), \hat{t}_d, (\hat{e}_d, \hat{r}_d)), g_{[e]} \rangle$ . Finally,  $\hat{t}_d$  is regarded as the estimated arrival time. Figure 6(a) provides an example of the above procedure.

**4.5.2 Trajectory Recovery (TR).** This task aims to recover a sparse trajectory’s dense counterpart. The proposed model can handle this task using a similar procedure as described in Section 4.4.1. The only difference is that the spans can be generated in their original order without shuffling. Whether a sub-trajectory between a pair of sparse trajectory’s consecutive points is absent can be deduced from the sampling interval. Specifically, suppose we have two trajectory points  $(l_i, t_i)$  and  $(l_{i+1}, t_{i+1})$  from a sparse trajectory, and a desired sampling interval  $\eta$  for the recovered dense trajectory. If  $t_{i+1} - t_i > \eta$  then we insert the tuple  $g_{[m]}$  between these two points, indicating that there is an absent sub-trajectory to be generated.

**4.5.3 Trajectory Prediction (TP).** This task aims to predict future trajectory points given historical ones. Suppose the first  $n$  points of a trajectory  $\mathcal{T}$  are known. The model is provided with an input sequence  $\langle g_1^{\mathcal{T}}, \dots, g_n^{\mathcal{T}}, g_{[m]} \rangle$ . Next, the model generates the span of future tuples corresponding to  $g_{[m]}$  following the procedure outlined in Section 4.2.2. The generated span can be expressed as  $\langle \hat{g}_{n+1}^{\mathcal{T}}, \hat{g}_{n+2}^{\mathcal{T}}, \dots, \hat{g}_N^{\mathcal{T}}, g_{[e]} \rangle$ , where  $N$  is the length of the trajectory. An example of the above procedure is illustrated in Figure 6(b).

The model can be directly applied to a task post pre-training in a zero-shot manner by providing the model with the task-specific input arrangements detailed above. In our experiments, fine-tuning with task-specific generations is conducted post pre-training to further improve the model’s performance on tasks. Subsequent sections will delve into the comparison of performance between fine-tuned and non-fine-tuned models, the rate of convergence in fine-tuning, and the scalability of the fine-tuning dataset.

## 5 EXPERIMENTS

To access the performance of the proposed model, we conduct experiments on two real-world trajectory datasets under varying experimental settings.

### 5.1 Datasets

We conduct experiments using two datasets: Chengdu and Porto. These datasets consist of taxi trajectories from Chengdu, China, and Porto, Portugal, respectively. The Chengdu dataset was released by Didi<sup>1</sup> and consists of GPS trajectories of taxis operating in Chengdu. The Porto dataset was released on Kaggle<sup>2</sup> for a taxi trajectory prediction contest. We also fetch the road network of Chengdu and Porto from OpenStreetMap<sup>3</sup> for map-matching. For consistency in our analyses, these datasets are both standardized to a sampling interval of 15 seconds. Trajectories that feature fewer than 6 points, being relatively short, are excluded from our study. An overview of dataset statistics can be found in Table 1.

Table 1: Dataset statistics.

Dataset	Chengdu	Porto
Time span	10.01–11.30, 2018	07.01–09.01, 2013
Longitude scope	104.04300~104.12654	-8.65200~8.57801
Latitude scope	30.65523~30.72699	41.14201~41.17399
Number of road segments	2,505	2,225
Number of trajectories	121,394	55,120
Number of points	3,032,212	1,482,751

### 5.2 Comparison Methods

To assess the performance of the proposed model across the three trajectory-related tasks outlined in Section 4.5, we benchmark its performance against a variety of state-of-the-art methods. These include both general trajectory models and methods specifically designed for the tasks at hand.

**5.2.1 Travel Time Estimation Methods.** We benchmark the performance of the proposed model on the TTE task against the following origin-destination travel time estimation methods.

- **RNE** [20]: determines the path distances between road segments by referencing their latent embeddings.
- **TEMP** [41]: calculates the mean travel times of historical trajectories that align closely in terms of locations and time.
- **LR**: establishes a linear mapping from input features to travel times based on training labels.

<sup>1</sup><https://gaia.didichuxing.com/>

<sup>2</sup><https://www.kaggle.com/competitions/pkdd-15-predict-taxi-service-trajectory-i/data>

<sup>3</sup><https://www.openstreetmap.org/>

- **GBM**: an advanced non-linear regression model, which we implement via XGBoost [3].
- **ST-NN** [22]: concurrently predicts both travel distances and travel times for OD pairs.
- **MURAT** [27]: jointly predicts travel distance and time while utilizing the departure time as extra information.
- **DeepOD** [53]: exploits the correlation between input features and historical trajectories during training.
- **DOT** [30]: a two-stage framework that generates an image representation of trajectories for estimating travel time.

5.2.2 *Trajectory Recovery Methods*. We compare the proposed model on the TR task against the following trajectory recovery methods, including both non-learning-based and learning-based approaches.

- **Shortest Path** [1]: recovers paths between consecutive points in sparse trajectories with Dijkstra’s shortest path algorithm [23] on road networks.
- **Linear** [19]: extends sparse trajectories using linear interpolation.
- **TrImpute** [8]: imputes sparse trajectories with a crowd wisdom-based algorithm.
- **DHTR** [42]: combines the seq2seq framework [36] and Kalman filtering to recover dense trajectories.
- **AttnMove** [45]: leverages Attention mechanisms to predict the sequence of road segments.
- **MTrajRec** [35]: employs a GRU-based auto-regressive model to recover road network-constrained trajectories.
- **RNTRajRec** [5]: integrates the transformer model and the inherent road network structure to recover trajectories.

5.2.3 *Trajectory Prediction Methods*. The following trajectory prediction methods for comparison encompass both models specifically designed for the TP task, as well as general trajectory models. To generate predictions, a prediction module implemented with fully-connected network is incorporated into the embedding vectors produced by these general trajectory models.

- **trajectory2vec** [52]: constructs behavior sequences to extract high-level correlations in trajectories.
- **t2vec** [26]: builds upon an auto-encoding framework, offering a more robust general trajectory model.
- **DeepMove** [11]: an end-to-end Attentional RNN-based sequential model designed for predicting future movements.
- **Transformer** [39]: a widely-used sequential model that excels at extracting correlations in long sequences.
- **Trembr** [13]: integrates road network information with auto-encoding for general trajectory modeling.
- **START** [21]: incorporates both spatio-temporal correlations and travel semantics for general trajectory modeling.

It is noteworthy that *Trembr* and *START* require road segment features for optimal functioning, which are not directly obtainable in the context of sparse trajectories. Therefore, the trajectories recovered by the most effective TR baseline, RNTRajRec, are served as input to them during evaluation. These combinations are denoted as *Trembr+RNTR* and *START+RNTR*. We also report their performance when they are fed with map-matched, real dense trajectories.

5.2.4 *Variations without pre-training or fine-tuning*. To further assess the effectiveness of the pre-training and fine-tuning processes within the proposed model, we introduce two additional variations for comparison.

- **GTM w/o pt**: excludes the pre-training process in Section 4.4, and supervises the model solely with task-specific generation.
- **GTM w/o ft**: bypasses the fine-tuning process. After pre-training the model, directly employs it to handle tasks with task-specific input arrangements in a zero-shot manner.

### 5.3 Settings

In both datasets, trajectories are initially sorted by departure time, and then they are divided into training, validation, and testing sets with ratios of 8:1:1. All methods undergo training using the training set, and the validation set is employed for hyper-parameter tuning and early stopping. The final metrics are derived from the testing set. For the TR and TP tasks, three sampling intervals are used, i.e., 1, 2, and 4 minutes, to simulate different levels of sparsity in trajectories. The TR task aims to recover these sparse trajectories into dense ones with a 15-second sampling interval. The TP task aims to predict the road segments, fraction, coordinates, and times of the trajectories’ destinations, given historical trajectories except their last points.

To quantify the performance of the different approaches, we employ different metrics for the three downstream tasks. 1) *For the TR task*, following MTrajRec [35], the Precision and Recall of the recovered road segments are determined. Specifically, for each evaluation sample, we gather the set  $\mathcal{E}_R$  of recovered road segments and the set  $\mathcal{E}_G$  of ground truth road segments from the road segment features. Then, the Precision is calculated as  $\frac{|\mathcal{E}_R \cap \mathcal{E}_G|}{|\mathcal{E}_R|}$ , and the Recall is calculated as  $\frac{|\mathcal{E}_R \cap \mathcal{E}_G|}{|\mathcal{E}_G|}$ . Additionally, the mean absolute error (MAE) of distances for the recovered coordinates and road locations is determined. The distance between a pair of recovered and ground truth trajectory points is determined either by their shortest distance on the Earth’s surface or the road network, depending on whether we are evaluating the recovered coordinates or road locations. 2) *For the TP task*, we report the Accuracy of the predicted road segment indices, the distance MAE of the predicted coordinates and road locations, and the MAE of the predicted time. 3) *For the TTE task*, we use the root mean squared error (RMSE), MAE, and the mean absolute percentage error (MAPE) to evaluate the accuracy of estimated travel times.

All methods are implemented using Python and PyTorch [33]. Baselines are configured according to the optimal parameter settings suggested in their respective papers. Three key hyper-parameters in the proposed model are considered during experiments, with their ranges and optimal values reported in Table 2.

Table 2: Hyper-parameter range and optimal values.

Parameter	Range
$d$	32, 64, <u>128</u> , 192, 256
$N_h$	1, 2, 4, <u>8</u> , 16
$\delta$ (meters)	10, 50, <u>100</u> , 150, 200

## 5.4 Comparison with Baselines

**5.4.1 Comparison on Overall Accuracy.** Tables 3, 4, and 5 present the performance results of different approaches for the TTE, TR, and TP tasks, respectively. The results indicate that the proposed model is capable of consistently outperforming comparison methods on diverse trajectory-related tasks, demonstrating its adaptability.

For the TTE task, the proposed model performs better than the state-of-the-art baseline, *DOT*, owing to its pre-training that enhances its understanding of the correlations between trajectories and travel times. The superiority is further substantiated by the fact that while *DOT* outperforms *GTM w/o pt*, it still lags behind the pre-trained and fine-tuned *GTM*.

For the TR task, a limitation associated with the comparison methods is that they are typically trained to fit sparse trajectories with a specific sampling interval, thereby constraining their generalizability. In contrast, the proposed model, by leveraging pre-training, can adapt to trajectories with varying sampling intervals without necessitating complete re-training. The performance of *GTM w/o ft* shows that the model can match or even exceed the best-performing baselines without fine-tuning, emphasizing its robustness to varying sampling intervals.

For the TP task, while *Trembr* and *START* are effective in modeling dense trajectories, their performance decreases notably with sparse trajectories. Pairing them with TR methods does not yield optimal results due to the accumulation of errors in this configuration. In contrast, the proposed model is tailored to accommodate sparsity, resulting in excellent performance even when faced with sparse trajectories. Table 6 demonstrates that the proposed model, utilizing sparse trajectories sampled at 1-minute intervals, can even outperform *Trembr* and *START* fed with dense trajectories sampled at 15-second intervals.

**5.4.2 Comparison on Efficiency.** We assess the efficiency of the different approaches across three dimensions: model size, training time, and testing time. The model size reflects the memory requirements during operation, while the training and testing time

**Table 3: Travel time estimation accuracy comparison of different approaches.**

Datasets		Chengdu / Porto		
Methods		MAE (min) ↓	RMSE (min) ↓	MAPE (%) ↓
RNE		1.087 / 2.357	4.967 / 7.168	18.185 / 53.894
TEMP		0.816 / 2.610	1.100 / 3.414	13.003 / 59.178
LR		0.815 / 2.596	1.097 / 3.408	12.997 / 58.390
GBM		0.773 / 2.200	1.202 / 3.116	11.142 / 43.308
ST-NN		0.770 / 2.136	1.031 / 3.027	12.470 / 45.285
MURAT		0.731 / 1.971	0.979 / 2.827	11.931 / 41.259
DeepOD		0.640 / 1.899	0.880 / 2.780	10.517 / 36.956
<b>DOT</b>		<u>0.614</u> / <u>1.777</u>	<u>0.841</u> / <u>2.644</u>	<u>9.937</u> / <u>34.883</u>
GTM w/o pt		0.666 / 1.871	0.933 / 2.797	10.501 / 34.895
GTM w/o ft		2.203 / 3.470	2.469 / 4.694	35.039 / 45.700
<b>GTM</b>		<b>0.561</b> / <b>1.615</b>	<b>0.784</b> / <b>2.470</b>	<b>8.853</b> / <b>31.391</b>

**Bold** denotes the best result, underline denotes the second-best result. ↓ means lower is better.

provide insights into the efficiency during training and testing. The calculations for model sizes are determined based on the types and numbers of learnable parameters of each approach. Furthermore, the training and testing times are recorded on a machine equipped with an Intel(R) Xeon(R) Gold 5215 CPU and an nVidia(R) Quadro RTX 8000 GPU.

As detailed in Table 7, the proposed model exhibits similar or superior efficiency when compared with the leading methods for each task. Notably, in real-world scenarios where multiple tasks are performed on the same dataset, our model showcases even higher computational efficiency compared to existing solutions. This is because our model can be trained once and perform different tasks, while existing solutions require separate training and storage for each task. For instance, to execute the TTE, TR, and TP tasks on the Chengdu dataset, opting for state-of-the-art baselines would necessitate a training time of 20.675 minutes per epoch. In comparison, training our model only requires 1.668 minutes per epoch.

## 5.5 Performance Analysis

**5.5.1 Efficacy of Pre-training.** The advantage of pre-training is assessed by comparing the convergence rate of the proposed model on tasks when employed with and without pre-training. Specifically, we track the performance metrics of the proposed model on tasks across training epochs. The findings are shown in Figure 7.

The observations are clear: across both TR and TP tasks, the pre-trained model consistently outperforms its non-pre-trained counterpart in terms of convergence rate. This demonstrates the model's capability to smoothly transition between different tasks with minimal fine-tuning. By achieving superior performance in fewer epochs, the pre-training process enhances computational efficiency, particularly in situations where a single dataset is utilized for multiple tasks.

**5.5.2 Scalability of Pre-training with Limited Data.** The construction of pre-training samples in the proposed model requires a certain amount of densely sampled trajectories. Thus, it is of interest to determine how effectively the model operates when faced with limited dense trajectories. To assess this aspect, we examine the scalability of the model in scenarios where only a subset of the training dense trajectories is available for the pre-training phase.

The results in Figure 8 offer several insights. Notably, the proposed model exhibits strong consistency. Even when the pre-training is performed with limited data, the performance remains relatively robust. This underscores the model's potential in practical contexts where obtaining large-scale dense trajectories might pose challenges. Furthermore, a significant improvement in performance is evident when comparing the results at 20% scale to those of the model without any pre-training (0% scale). This is further evidence of the benefits of the pre-training.

**5.5.3 Scalability of Fine-tuning with Limited Task-specific Data.** Comparing the model's performance with and without fine-tuning in both Tables 3 and 5, reveals a clear advantage when fine-tuning is applied. This can be credited to the difference in input arrangements between pre-training and specific tasks. Such a marked difference raises the question: does the model rely on extensive fine-tuning datasets to achieve optimal performance?

**Table 4: Trajectory recovery accuracy comparison of different approaches.**

Sampling Interval $\mu$		1 minute / 2 minutes / 4 minutes			
Datasets	Methods	Precision (%) $\uparrow$	Recall (%) $\uparrow$	MAE (Coor, meters) $\downarrow$	MAE (Road, meters) $\downarrow$
Chengdu	Shortest Path	62.638 / 43.504 / 29.431	59.346 / 40.949 / 27.607	213.10 / 428.69 / 752.19	206.91 / 391.39 / 586.09
	Linear	66.642 / 48.604 / 36.209	65.557 / 45.234 / 30.496	183.64 / 385.23 / 675.85	169.46 / 378.96 / 564.19
	TrImpute	77.520 / 60.179 / 57.526	76.202 / 58.461 / 53.747	166.82 / 276.56 / 408.64	155.71 / 265.34 / 387.36
	DHTR	53.514 / 53.608 / 50.985	58.868 / 47.918 / 46.311	205.59 / 317.45 / 450.61	300.67 / 470.46 / 547.41
	AttnMove	84.162 / 81.402 / 78.645	81.839 / 76.612 / 69.257	252.59 / 280.20 / 354.39	201.51 / 258.69 / 323.52
	MTrajRec	85.039 / 82.596 / <u>80.684</u>	83.351 / 80.113 / <u>72.952</u>	243.01 / 264.15 / <u>311.53</u>	173.67 / 204.58 / <u>282.88</u>
	RNTRajRec	87.653 / 83.174 / 79.404	<u>86.025</u> / <u>80.150</u> / 72.633	215.24 / 234.27 / 326.92	114.04 / <u>148.04</u> / 292.61
	GTM w/o pt	83.720 / 77.425 / 72.471	82.827 / 73.933 / 62.757	194.30 / 272.86 / 479.49	86.15 / 230.68 / 448.98
Porto	GTM w/o ft	<u>87.664</u> / <u>83.592</u> / 79.096	85.837 / 78.406 / 70.717	<u>137.69</u> / <u>217.85</u> / 350.29	<u>81.81</u> / 167.16 / 315.07
	<b>GTM</b>	<b>89.071</b> / <b>84.373</b> / <b>80.828</b>	<b>88.249</b> / <b>81.520</b> / <b>73.212</b>	<b>133.38</b> / <b>192.54</b> / <b>304.72</b>	<b>67.98</b> / <b>143.48</b> / <b>275.37</b>
	Shortest Path	69.780 / 53.590 / 40.492	60.354 / 46.263 / 33.758	202.17 / 434.37 / 679.72	165.02 / 319.32 / 478.66
	Linear	72.961 / 60.966 / 48.529	63.146 / 48.401 / 35.507	196.51 / 403.05 / 621.88	132.76 / 275.43 / 430.22
Porto	TrImpute	76.781 / 66.492 / 50.021	69.599 / 58.676 / 43.052	132.76 / 275.43 / 430.22	128.48 / 235.63 / 347.30
	DHTR	63.287 / 58.897 / 52.658	62.511 / 56.444 / 42.462	235.32 / 292.65 / 355.23	285.68 / 336.48 / 389.18
	AttnMove	79.541 / 75.751 / 71.248	67.116 / 56.751 / 48.991	184.70 / 222.51 / 304.31	134.17 / 184.03 / 251.92
	MTrajRec	78.081 / 72.847 / 64.566	71.853 / 60.068 / 46.110	168.34 / 283.90 / 496.96	121.64 / 215.40 / 391.67
	RNTRajRec	80.305 / 77.094 / <u>75.573</u>	74.953 / <u>65.370</u> / <u>50.965</u>	135.17 / <u>175.42</u> / <u>294.08</u>	111.75 / 152.49 / <b>230.30</b>
	GTM w/o pt	81.058 / 73.842 / 67.189	77.683 / 61.987 / 42.688	132.97 / 229.11 / 496.99	<u>69.70</u> / 204.01 / 488.13
	GTM w/o ft	<u>81.716</u> / <u>79.067</u> / 74.732	<u>75.144</u> / 63.059 / 50.269	<u>118.79</u> / 194.37 / 338.30	76.46 / <u>159.81</u> / 320.79
	<b>GTM</b>	<b>82.640</b> / <b>79.494</b> / <b>77.068</b>	<b>78.605</b> / <b>66.850</b> / <b>53.436</b>	<b>103.06</b> / <b>164.75</b> / <b>282.61</b>	<b>63.18</b> / <b>138.66</b> / <b>268.98</b>

**Bold** denotes the best result, and underline denotes the second-best result.  $\uparrow$  means higher is better, and  $\downarrow$  means lower is better.

**Table 5: Trajectory prediction accuracy comparison of different approaches.**

Sampling Interval $\mu$		1 minute / 2 minutes / 4 minutes			
Datasets	Methods	Accuracy (%) $\uparrow$	MAE (Coor, meters) $\downarrow$	MAE (Road, meters) $\downarrow$	MAE (Time, seconds) $\downarrow$
Chengdu	trajectory2vec	31.496 / 24.403 / 17.163	1514.5 / 1682.8 / 1861.6	1322.0 / 1616.5 / 1957.5	14.474 / 20.722 / 37.256
	t2vec	53.349 / 43.303 / 35.058	528.65 / 602.45 / 731.00	286.18 / 434.27 / 635.45	13.016 / 19.539 / 34.488
	DeepMove	58.499 / 45.985 / 37.338	<u>319.14</u> / 461.73 / 664.93	258.96 / 397.95 / 607.42	11.994 / 19.435 / 35.039
	Transformer	65.192 / 60.028 / <u>55.139</u>	374.36 / <u>402.11</u> / <u>431.01</u>	236.86 / <u>287.61</u> / <u>320.92</u>	16.287 / 29.848 / 34.226
	Trembr+RNTR	52.065 / 43.196 / 34.655	421.95 / 482.67 / 561.89	398.76 / 455.98 / 532.03	14.346 / 19.110 / 28.659
	START+RNTR	59.462 / 48.466 / 40.941	375.39 / 421.45 / 481.32	355.00 / 399.66 / 457.35	12.771 / 14.439 / 19.443
	GTM w/o pt	<u>71.795</u> / 50.041 / 33.882	376.05 / 540.89 / 857.43	263.83 / 568.73 / 942.64	<u>5.301</u> / <u>10.198</u> / <u>9.562</u>
	GTM w/o ft	<u>67.064</u> / <u>61.766</u> / 53.949	368.30 / 452.75 / 544.02	<u>230.24</u> / 320.19 / 443.43	6.084 / 12.189 / 9.910
	<b>GTM</b>	<b>82.820</b> / <b>78.921</b> / <b>72.083</b>	<b>260.31</b> / <b>303.44</b> / <b>362.32</b>	<b>128.44</b> / <b>200.80</b> / <b>260.13</b>	<b>3.821</b> / <b>7.919</b> / <b>7.131</b>
Porto	trajectory2vec	13.396 / 10.178 / 5.440	1709.3 / 2108.9 / 2488.5	2227.4 / 2425.6 / 3003.6	31.442 / 46.097 / 54.585
	t2vec	38.945 / 30.805 / 22.812	432.77 / 528.89 / 732.13	206.95 / 346.72 / 641.26	17.420 / 28.436 / 48.651
	DeepMove	43.774 / 33.562 / 23.645	<u>252.22</u> / 390.57 / 679.62	197.89 / 328.93 / 681.40	16.998 / 26.309 / 46.629
	Transformer	43.441 / 39.425 / 33.685	323.58 / <u>351.18</u> / <u>402.32</u>	216.18 / 256.89 / 283.72	18.231 / 30.541 / 49.083
	Trembr+RNTR	40.128 / 34.857 / 26.004	413.20 / 471.45 / 620.77	393.18 / 448.74 / 597.73	18.915 / 21.843 / 28.683
	START+RNTR	52.118 / 43.617 / 34.931	351.98 / 416.83 / 503.32	333.56 / 396.39 / 483.41	14.729 / 17.722 / 22.455
	GTM w/o pt	<u>61.480</u> / 46.938 / 31.304	307.23 / 369.86 / 649.71	<u>145.36</u> / 295.58 / 624.11	<u>10.853</u> / <u>11.316</u> / <u>11.643</u>
	GTM w/o ft	<u>48.770</u> / <u>48.474</u> / <u>44.477</u>	325.58 / 370.04 / 454.70	170.32 / <u>193.40</u> / <u>279.12</u>	11.509 / 18.342 / 18.081
	<b>GTM</b>	<b>68.529</b> / <b>67.697</b> / <b>65.125</b>	<b>238.83</b> / <b>232.15</b> / <b>322.63</b>	<b>99.67</b> / <b>103.79</b> / <b>140.17</b>	<b>6.845</b> / <b>9.449</b> / <b>11.549</b>

**Bold** denotes the best result, and underline denotes the second-best result.  $\uparrow$  means higher is better, and  $\downarrow$  means lower is better.

**Table 6: Trajectory prediction accuracy comparison between baselines fed with dense trajectories and the proposed model.**

Datasets		Chengdu / Porto		
Methods	$\mu$	Accuracy (%)	MAE (Coor, m.)	MAE (Time, sec.)
Trembr	15 sec.	66.077 / 52.063	399.40 / 362.84	8.534 / 15.046
START	15 sec.	74.990 / 62.997	354.76 / 318.26	8.068 / 12.476
<b>GTM</b>	<b>4 min.</b>	72.083 / <u>65.125</u>	362.32 / 322.63	<u>7.131</u> / 11.549
<b>GTM</b>	<b>1 min.</b>	<b>82.820</b> / <b>68.529</b>	<b>260.31</b> / <b>238.83</b>	<b>3.821</b> / <b>6.845</b>

**Bold** denotes the best result, underline denotes the second-best result.

**Table 7: Efficiency metrics of different approaches.**

Datasets		Chengdu / Porto		
Tasks	Methods	Model size (MBytes)	Train time (min/epoch)	Test time (sec)
TTE	RNE	2.446 / 2.173	0.100 / 0.040	0.170 / 0.062
	ST-NN	1.185 / 1.185	0.112 / 0.082	0.220 / 0.085
	MURAT	9.120 / 8.847	0.153 / 0.095	0.210 / 0.075
	DeepOD	8.184 / 7.928	0.382 / 0.171	0.328 / 0.099
	DOT	8.763 / 8.496	1.552 / 0.752	1.672 / 0.926
	<b>GTM</b>	10.146 / 9.333	0.533 / 0.336	1.231 / 0.647
TR	TrImpute	2.778 / 1.262	- / -	6.110K / 2.199K
	DHTR	6.426 / 6.426	0.176 / 0.115	2.503K / 0.257K
	AttnMove	6.799 / 6.250	6.844 / 2.460	92.673 / 32.081
	MTrajRec	19.180 / 18.495	8.470 / 4.437	0.125K / 54.062
	RNTRajRec	20.639 / 19.876	8.925 / 4.463	0.144K / 60.861
	<b>GTM</b>	10.146 / 9.333	1.668 / 1.470	21.984 / 15.237
TP	trajectory2vec	6.306 / 6.306	0.158 / 0.085	0.204 / 0.110
	t2vec	7.170 / 7.170	0.278 / 0.109	0.221 / 0.113
	DeepMove	5.282 / 5.282	0.253 / 0.126	0.567 / 0.292
	Transformer	6.295 / 6.295	1.090 / 0.538	3.568 / 1.596
	Trembr+RNTR	26.103 / 25.792	9.468 / 5.072	0.149K / 62.500
	START+RNTR	28.708 / 27.099	10.198 / 5.420	0.158K / 65.468
	<b>GTM</b>	10.146 / 9.333	1.667 / 1.450	3.357 / 1.703

To answer the question, we investigate the model’s scalability under scenarios where only a fraction of the task-specific data is available for fine-tuning. It is clear from the results in Figure 9 that the proposed model exhibits a remarkable stability at approximating its best performance when given just 20% of the full fine-tuning datasets. Comparing these results against a scenario where no fine-tuning is performed (0% scale), we see that even a minuscule fine-tuning dataset can facilitate the model to improve its accuracy on tasks. These findings underscore the model’s utility in the real-world, where gathering large-scale task-specific labeled datasets can be challenging.

**5.5.4 Effectiveness of Hyper-parameters.** We analyze the influence of the three primary hyper-parameters in Table 2 on the performance of the model. The results are presented in Figure 10. We highlight the following observations:

- (1) The embedding dimensionality  $d$  determines the expressive power of the model. As evident from Figure 10(a), an increase in  $d$  typically yields improved performance. However, beyond  $d = 128$ , the gains in performance are marginal, while the computational and memory overheads continue to grow. Therefore,

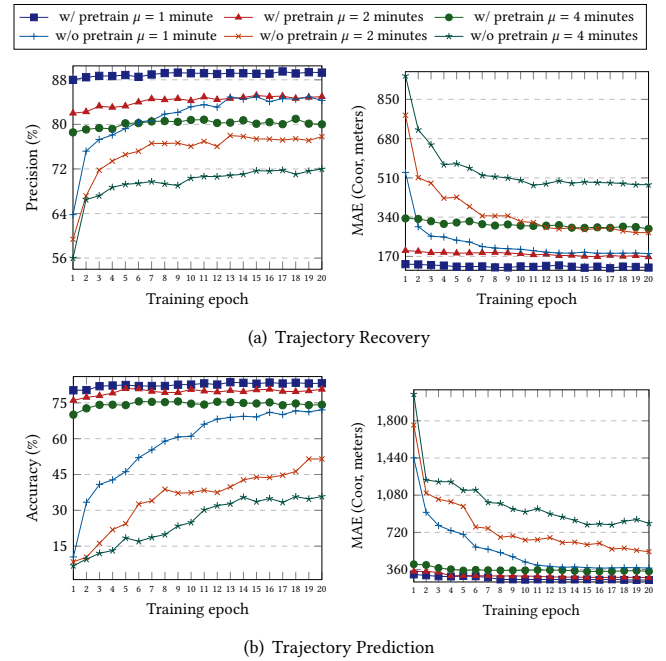


**Figure 7: Comparison of convergence rate with or without pre-training in Chengdu.**

$d = 128$  appears to be an ideal trade-off between performance and computational efficiency.

- (2) The number of Attention heads  $N_h$  controls the representational capacity of the encoder in our model. Drawing from Figure 10(b), the most beneficial value of both Precision and MAE occur at  $N_h = 8$ .
- (3) The distance threshold  $\delta$  determines the spatial scope of road segment neighbors. The insights from Figure 10(c) suggest its primary effect is on the precision of the generated road segments, with minimal influence on the accuracy of predicted coordinates. A peak in Precision is observed at  $\delta = 100$ . Employing a smaller threshold might result in missed road segment candidates, while a larger threshold can introduce more noise into the generation progress.
- 5.5.5 Effectiveness of Modules.** To determine the impact of individual features and modules in the proposed model, we conduct an ablation study. This involves contrasting the performance of the complete model with the performance of the following variations.
  - (1) *w/o neigh.*: excludes the set of road segment neighbors  $\Omega(l_i)$  in Equation 1.
  - (2) *w/o coor.*: excludes the coordinate feature  $l_i$  in Equation 1.
  - (3) *w/o time*: excludes the time feature  $t_i$  in Equation 1.
  - (4) *w/o shuffle*: does not shuffle the order of generated spans during the pre-training procedure.
  - (5) *Flat encoder*: calculates  $h_i$  as the mean pooling of  $Z_i$  instead of using self-attention.
  - (6) *FC num. enc.*: replaces the encoding module  $\Phi$  with a fully connected network.

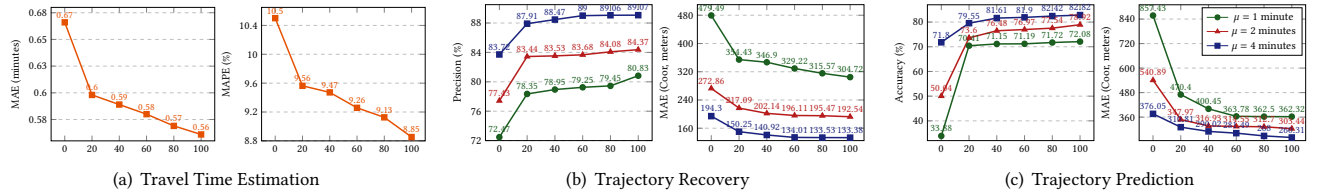


Figure 8: Scalability with regard to the size (%) of pre-train sets in Chengdu.

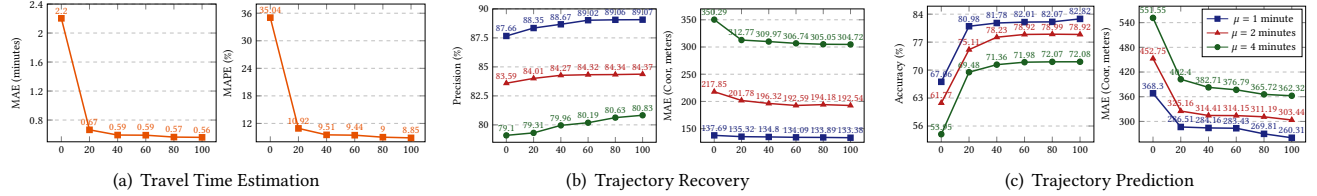


Figure 9: Scalability with regard to the size (%) of fine-tune sets in Chengdu.

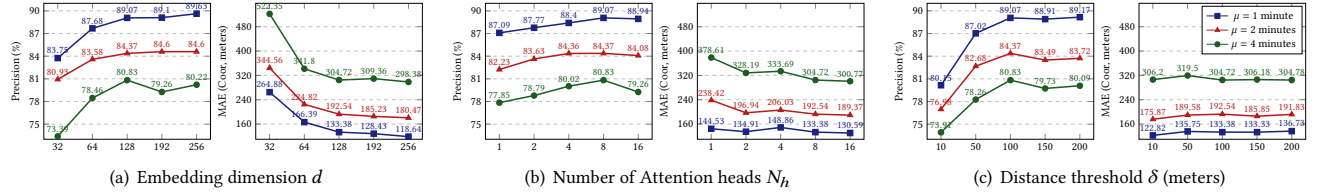


Figure 10: Effectiveness of hyper-parameters on the trajectory recovery task in Chengdu.

Table 8: Effectiveness of features and modules on the sparse trajectory recovery task in Chengdu.

Sampling Interval $\mu$	1 minute / 2 minutes / 4 minutes
Variations	Precision (%) MAE (Coor, meters)
w/o neigh.	76.834 / 74.494 / 71.950
w/o coor.	78.891 / 77.345 / 72.433
w/o time	86.821 / 83.230 / 77.055
w/o shuffle	84.406 / 77.467 / 73.589
Flat encoder	85.548 / 79.874 / 74.162
FC num. enc.	86.051 / 81.433 / 76.964
GTM	89.071 / 84.343 / 80.828

The results are computed on Chengdu’s test set for the TR task, as shown in Table 8. We draw the following observations:

- (1) The road segment neighbors, coordinates, and time features collectively enhance the efficacy of the model. Excluding any of these features yields a noticeable drop in performance.
- (2) Omitting shuffling when performing pre-training limits the model’s ability to capture bi-directional correlations in trajectories, causing a decline in performance.
- (3) The hierarchical attention in the trajectory encoder and the encoding module in the feature domain embedding layer are effective at enhancing the model’s performance.

## 6 CONCLUSION

In this paper, we introduce GTM, a versatile and robust general trajectory model. GTM is distinguished by its ability to be trained once on a given dataset and subsequently adapt to a variety of trajectory-related tasks without relying on additional prediction modules. To ensure its applicability across diverse tasks, GTM separates features in trajectories into three distinct domains, allowing for the independent masking and generation of each domain to accommodate the unique input and output needs of different tasks. Furthermore, GTM’s robustness to sparsity is enhanced through a pre-training process. During this process, GTM learns to reconstruct the feature domains of densely sampled trajectories from their re-sampled sparse counterparts, thus maintaining its performance in the presence of sparsity. The versatility and robustness of GTM are able to improve both computational and storage efficiency in ITS, facilitating the execution of multiple tasks with a single model and enabling efficient dataset downsizing through re-sampling. Empirical evaluation on two real-world trajectory datasets and three representative tasks demonstrates GTM’s superior performance, proving GTM’s effectiveness in achieving its objective of general trajectory modeling.

## ACKNOWLEDGMENTS

This work was supported by the National Natural Science Foundation of China (No. 62272033).

## REFERENCES

[1] Erin W. Chambers, Brittany Terese Fasy, Yusu Wang, and Carola Wenk. 2020. Map-Matching Using Shortest Paths. *ACM Trans. Spatial Algorithms Syst.* 6, 1 (2020), 6:1–6:17.

[2] Pingfu Chao, Yehong Xu, Wen Hua, and Xiaofang Zhou. 2020. A Survey on Map-Matching Algorithms. In *ADC (Lecture Notes in Computer Science)*, Vol. 12008. 121–133.

[3] Tianqi Chen and Carlos Guestrin. 2016. Xgboost: A scalable tree boosting system. In *KDD*. 785–794.

[4] Ting Chen, Simon Kornblith, Mohammad Norouzi, and Geoffrey E. Hinton. 2020. A Simple Framework for Contrastive Learning of Visual Representations. In *ICML*, Vol. 119. 1597–1607.

[5] Yuqi Chen, Hanyuan Zhang, Weiwei Sun, and Baihua Zheng. 2023. Rntrajrec: Road network enhanced trajectory recovery with spatial-temporal transformer. (2023), 829–842.

[6] Jacob Devlin, Ming-Wei Chang, Kenton Lee, and Kristina Toutanova. 2019. BERT: Pre-training of Deep Bidirectional Transformers for Language Understanding. In *NAACL-HLT*. 4171–4186.

[7] Zhengxiao Du, Yujie Qian, Xiao Liu, Ming Ding, Jiezhong Qiu, Zhilin Yang, and Jie Tang. 2022. GLM: General Language Model Pretraining with Autoregressive Blank Infilling. In *ACL*. 320–335.

[8] Mohamed M. Elshrif, Keivin Isufaj, and Mohamed F. Mokbel. 2022. Network-less trajectory imputation. In *SIGSPATIAL*. 8:1–8:10.

[9] Ziquan Fang, Shenghao Gong, Lu Chen, Jiachen Xu, Yunjun Gao, and Christian S. Jensen. 2023. Ghost: A General Framework for High-Performance Online Similarity Queries over Distributed Trajectory Streams. *Proc. ACM Manag. Data* 1, 2 (2023), 173:1–173:25.

[10] Ziquan Fang, Lu Pan, Lu Chen, Yuntao Du, and Yunjun Gao. 2021. MDTP: A Multi-source Deep Traffic Prediction Framework over Spatio-Temporal Trajectory Data. *Proc. VLDB Endow.* 14, 8 (2021), 1289–1297.

[11] Jie Feng, Yong Li, Chao Zhang, Funing Sun, Fanchao Meng, Ang Guo, and Depeng Jin. 2018. DeepMove: Predicting Human Mobility with Attentional Recurrent Networks. In *WWW*. 1459–1468.

[12] Kun Fu, Fanlin Meng, Jieping Ye, and Zheng Wang. 2020. CompactETA: A Fast Inference System for Travel Time Prediction. In *KDD*. 3337–3345.

[13] Tao-Yang Fu and Wang-Chien Lee. 2020. Trembr: Exploring Road Networks for Trajectory Representation Learning. *ACM Trans. Intell. Syst. Technol.* 11, 1 (2020), 10:1–10:25.

[14] Yunchong Gan, Haoyu Zhang, and Mingjie Wang. 2021. Travel Time Estimation Based on Neural Network with Auxiliary Loss. In *SIGSPATIAL*. 642–645.

[15] Chenjuan Guo, Bin Yang, Jilin Hu, Christian S. Jensen, and Lu Chen. 2020. Context-aware, preference-based vehicle routing. *VLDB J.* 29, 5 (2020), 1149–1170.

[16] Xiaolin Han, Reynold Cheng, Chenhao Ma, and Tobias Grubenmann. 2022. DeepTEA: Effective and Efficient Online Time-dependent Trajectory Outlier Detection. *Proc. VLDB Endow.* 15, 7 (2022), 1493–1505.

[17] Geoffrey E Hinton and Ruslan R Salakhutdinov. 2006. Reducing the dimensionality of data with neural networks. *science* 313, 5786 (2006), 504–507.

[18] Sepp Hochreiter and Jürgen Schmidhuber. 1997. Long short-term memory. *Neural computation* 9, 8 (1997), 1735–1780.

[19] Sahar Hoteit, Stefano Secci, Stanislav Sobolevsky, Carlo Ratti, and Guy Pujol. 2014. Estimating human trajectories and hotspots through mobile phone data. *Comput. Networks* 64 (2014), 296–307.

[20] Shuai Huang, Yong Wang, Tianyu Zhao, and Guoliang Li. 2021. A learning-based method for computing shortest path distances on road networks. In *ICDE*. 360–371.

[21] Jiawei Jiang, Dayan Pan, Houxing Ren, Xiaohan Jiang, Chao Li, and Jingyu Wang. 2022. Self-supervised Trajectory Representation Learning with Temporal Regularities and Travel Semantics. *CoRR* abs/2211.09510 (2022).

[22] Ishan Jindal, Zhiwei (Tony) Qin, Xue-wen Chen, Matthew S. Nokleby, and Jieping Ye. 2017. A Unified Neural Network Approach for Estimating Travel Time and Distance for a Taxi Trip. *CoRR* abs/1710.04350 (2017).

[23] Donald B Johnson. 1973. A note on Dijkstra's shortest path algorithm. *J. ACM* 20, 3 (1973), 385–388.

[24] Dejiang Kong and Fei Wu. 2018. HST-LSTM: A Hierarchical Spatial-Temporal Long-Short Term Memory Network for Location Prediction. In *IJCAI*. 2341–2347.

[25] Tianyi Li, Lu Chen, Christian S. Jensen, Torben Bach Pedersen, Yunjun Gao, and Jilin Hu. 2022. Evolutionary Clustering of Moving Objects. In *ICDE*. 2399–2411.

[26] Xiucheng Li, Kaiqi Zhao, Gao Cong, Christian S. Jensen, and Wei Wei. 2018. Deep Representation Learning for Trajectory Similarity Computation. In *ICDE*. 617–628.

[27] Yaguang Li, Kun Fu, Zheng Wang, Cyrus Shahabi, Jieping Ye, and Yan Liu. 2018. Multi-task representation learning for travel time estimation. In *KDD*. 1695–1704.

[28] Yang Li, Si Si, Gang Li, Cho-Jui Hsieh, and Samy Bengio. 2021. Learnable fourier features for multi-dimensional spatial positional encoding. *NeurIPS* 34 (2021), 15816–15829.

[29] Yuebing Liang and Zhan Zhao. 2022. NetTraj: A Network-Based Vehicle Trajectory Prediction Model With Directional Representation and Spatiotemporal Attention Mechanisms. *IEEE Trans. Intell. Transp. Syst.* 23, 9 (2022), 14470–14481.

[30] Yan Lin, Huaiyu Wan, Jilin Hu, Shengnan Guo, Bin Yang, Youfang Lin, and Christian S. Jensen. 2023. Origin-Destination Travel Time Oracle for Map-based Services. *SIGMOD* 1, 3 (2023), 1–27.

[31] Yiding Liu, Kaiqi Zhao, Gao Cong, and Zhifeng Bao. 2020. Online Anomalous Trajectory Detection with Deep Generative Sequence Modeling. In *ICDE*. 949–960.

[32] Congcong Miao, Ziyan Luo, Fengzhu Zeng, and Jilong Wang. 2020. Predicting Human Mobility via Attentive Convolutional Network. In *WSDM*. 438–446.

[33] Adam Paszke, Sam Gross, Francisco Massa, Adam Lerer, James Bradbury, Gregory Chanan, Trevor Killeen, Zeming Lin, Natalia Gimelshein, Luca Antiga, et al. 2019. PyTorch: An imperative style, high-performance deep learning library. In *NeurIPS*. 8024–8035.

[34] Simon Aagaard Pedersen, Bin Yang, and Christian S. Jensen. 2020. Anytime Stochastic Routing with Hybrid Learning. *Proc. VLDB Endow.* 13, 9 (2020), 1555–1567.

[35] Huimin Ren, Sijie Ruan, Yanhua Li, Jie Bao, Chuishi Meng, Ruiyuan Li, and Yu Zheng. 2021. MTrajRec: Map-Constrained Trajectory Recovery via Seq2Seq Multi-task Learning. In *KDD*. 1410–1419.

[36] Ilya Sutskever, Oriol Vinyals, and Quoc V. Le. 2014. Sequence to Sequence Learning with Neural Networks. In *NeurIPS*. 3104–3112.

[37] Matthew Tancik, Pratul Srinivasan, Ben Mildenhall, Sara Fridovich-Keil, Nithin Raghavan, Utkarsh Singhal, Ravi Ramamoorthi, Jonathan Barron, and Ren Ng. 2020. Fourier features let networks learn high frequency functions in low dimensional domains. *NeurIPS* 33 (2020), 7537–7547.

[38] Aäron van den Oord, Yazhe Li, and Oriol Vinyals. 2018. Representation Learning with Contrastive Predictive Coding. *CoRR* abs/1807.03748 (2018).

[39] Ashish Vaswani, Noam Shazeer, Niki Parmar, Jakob Uszkoreit, Llion Jones, Aidan N. Gomez, Łukasz Kaiser, and Illia Polosukhin. 2017. Attention is All you Need. In *NeurIPS*. 5998–6008.

[40] Dong Wang, Junbo Zhang, Wei Cao, Jian Li, and Yu Zheng. 2018. When will you arrive? Estimating travel time based on deep neural networks. In *AAAI*, Vol. 32. 2500–2507.

[41] Hongjian Wang, Xianfeng Tang, Yu-Hsuan Kuo, Daniel Kifer, and Zhenhui Li. 2019. A simple baseline for travel time estimation using large-scale trip data. *ACM Trans. on Intelli. Sys. and Tech.* 10, 2 (2019), 1–22.

[42] Jingyuan Wang, Ning Wu, Xinxin Lu, Wayne Xin Zhao, and Kai Feng. 2019. Deep trajectory recovery with fine-grained calibration using kalman filter. *IEEE Trans. on Knowl. and Data Eng.* 33, 3 (2019), 921–934.

[43] Zheng Wang, Kun Fu, and Jieping Ye. 2018. Learning to estimate the travel time. In *KDD*. 858–866.

[44] Fan Wu and Lixia Wu. 2019. DeepETA: a spatial-temporal sequential neural network model for estimating time of arrival in package delivery system. In *AAAI*, Vol. 33. 774–781.

[45] Tong Xia, Yunhan Qi, Jie Feng, Fengli Xu, Funing Sun, Diansheng Guo, and Yong Li. 2021. AttnMove: History Enhanced Trajectory Recovery via Attentional Network. In *AAAI*. 4494–4502.

[46] Bingqi Yan, Geng Zhao, Lexue Song, Yanwei Yu, and Junyu Dong. 2022. PreCLN: Pretrained-based contrastive learning network for vehicle trajectory prediction. *WWW* (2022), 1–23.

[47] Can Yang and Gyozo Gidofalvi. 2018. Fast map matching, an algorithm integrating hidden Markov model with precomputation. *Int. Journal of Geographical Information Science* 32, 3 (2018), 547–570.

[48] Ling Yang, Shouxu Jiang, and Fusheng Zhang. 2022. Multitask Learning with Graph Neural Network for Travel Time Estimation. *Computational Intelligence and Neuroscience* 2022 (2022).

[49] Sean Bin Yang, Chenjuan Guo, and Bin Yang. 2022. Context-Aware Path Ranking in Road Networks. *IEEE Trans. Knowl. Data Eng.* 34, 7 (2022), 3153–3168.

[50] Sean Bin Yang, Jilin Hu, Chenjuan Guo, Bin Yang, and Christian S. Jensen. 2023. LightPath: Lightweight and Scalable Path Representation Learning. In *KDD*. 2999–3010.

[51] Zhihui Yang, Zihang Dai, Yiming Yang, Jaime G. Carbonell, Ruslan Salakhutdinov, and Quoc V. Le. 2019. XLNet: Generalized Autoregressive Pretraining for Language Understanding. In *NeurIPS*. 5754–5764.

[52] Di Yao, Chao Zhang, Zhihua Zhu, Jian-Hui Huang, and Jingping Bi. 2017. Trajectory clustering via deep representation learning. In *IJCNN*. 3880–3887.

[53] Haitao Yuan, Guoliang Li, Zhifeng Bao, and Ling Feng. 2020. Effective Travel Time Estimation: When Historical Trajectories over Road Networks Matter. In *SIGMOD*. 2135–2149.

[54] Mingxuan Yue, Yaguang Li, Haoze Yang, Ritesh Ahuja, Yao-Yi Chiang, and Cyrus Shahabi. 2019. DETECT: Deep Trajectory Clustering for Mobility-Behavior Analysis. In *IEEE BigData*. 988–997.

[55] Fan Zhou, Yurou Dai, Qiang Gao, Pengyu Wang, and Ting Zhong. 2021. Self-supervised human mobility learning for next location prediction and trajectory classification. *Knowl. Based Syst.* 228 (2021), 107214.